A Plasma Model for Orificed Hollow Cathode

IEPC-2019-452

Presented at the 36th International Electric Propulsion Conference
University of Vienna, Austria
September 15-20, 2019

M. Panelli* , C. Giaquinto† , A. Smoraldi‡ and F. Battista§
CIRA, Italian Aerospace Research Center, Capua (CE), 81043, Italy

This paper presents the optimization of the zero-dimensional plasma models developed by CIRA for cathodes, obtained removing some of the previous models' assumptions. Particularly, Xenon electron-neutral cross section has been updated to consider only the elastic collisions: the proposed correlation agrees with the experimental data with an R-squared value of 0.99. The cathode internal total pressure, originally calculated using a theoretical approach, has been estimated by means of an empirical scaling relationship. The formula for the calculation of the internal plasma resistance has been revisited. A plasma model for the keeper region has been proposed, too. A LaB6 based emitter OHC fed by Xenon has been selected as baseline geometry to test the model. The trends of electron temperature, plasma densities, neutral densities and wall temperatures, as function of mass flow rate and discharge current, are in agreement with those reported in literature, as well as their distributions along the axis of the cathode. The electrical characteristic of the baseline cathode has been studied as function of mass flow rate at 3A and as function of the discharge current at 0.2 mg/s. The results have shown that the total voltage drops have been rebuilt with an accuracy ranging from 1 to 6% and from 5 to 14%, respectively. The effect of modeling a double sheath after the orifice exit has been also discussed. The results shows that the model can be used with 1÷5% of uncertainty when the cathode is operating in plume mode whereas the differences increase to ∼15% in spot mode.

Nomenclature

A = Area
L = Length
r = Radius
q = Elementary charge
k_B = Boltzmann's constant
I_d = Discharge current
j = Current density
J = Radiosity
K_i = Ionization rate coefficinet
m_e = Electron mass
m_i = Ion mass
$\dot{m}$ = Mass flow rate
n_e = Electron density

*Researcher, Methodologies and Technologies for Space Propulsion Lab., m.panelli@cira.it.
†Graduate Student, Methodologies and Technologies for Space Propulsion Lab., chiara.giaquinto1@studenti.unicampania.it.
‡Researcher, Propulsion Test Facilities Lab., a.smoraldi@cira.it.
§Head of Methodologies and Technologies for Space Propulsion Lab., f.battista@cira.it.

n_0	= Neutral density
$\dot{n}$	= Ion rate
p	= Pressure
P	= Power
R	= Resistence
T	= Temperature
T_e	= Electron temperature
V	= Potential
α	= Degree of ionization
η	= Plasma resistivity
ν	= Collision frequency
σ	= Coss section
γ	= Specific heat ratio
$\langle\epsilon_i\rangle$	= Average ionization energy loss

Subscripts

e	= emitter
o	= orifice
k	= keeper
en	= electron-neutral
ei	= electron-ion
i	= ion moving at Bohm speed
ion	= ionization
er	= electron recombination
em	= thermionic emission
$conv$	= convection
$cont$	= continuum flow
kin	= kinetic
th	= thermal
eff	= effective
s	= emitter surface
w	= wall
ds	= double sheath

I. Introduction

Thermionic hollow cathodes have been widely used in wide variety of areas such as spacecraft electric propulsion systems, material processing and lasers for more than half a century as efficient electron sources. Especially in electric propulsion systems, hollow cathodes are used as electron sources for propellant ionization and ion beam neutralization. The small geometry of the typical Orificed Hollow Cathodes (OHCs) make the plasma diagnostics difficult which is why numerical studies become important for understanding the driving physical processes behind their operation, and the effects of the geometry and the operation parameters on cathode performance.

At present, several global 0D models have been developed to determine the plasma properties in hollow cathodes[1,2,3,4] and also The Italian Aerospace Research Centre (CIRA), in the frame of the activities on space electric propulsion[5], is developing a tool to support the preliminary design of OHCs for research purpose[6,7].

The tool features plasma models validated by means of numerical and experimental cross checks [6,7] , but, being inspired by the existing ones[1,2,3,4], they suffered of inherited approximations which affects the handling of the cathodes' plasma physics[8].

Xenon electron-neutral collision frequency is usually[1,2,3] computed using the numerical fit to experimental data proposed by Katz *et al.*[9]. However this expression fits the total collision cross-section, which also includes inelastic collisions, instead of the more appropriate momentum transfer cross-section. Katz *et al.*'s correlation[9] approximates reasonably well the momentum transfer cross-section for electron temperatures between 0.8 and 2 eV whereas overestimates momentum transfer data by a factor of 2 for electron temperatures above 2 eV. More recent elastic electron-neutral cross-section data[10] also indicates that the fit underestimates the electron-neutral cross-section at low electron energies as shown in Ref. 8. For these reasons, retrieving the most recent elastic cross-section data from the LXCAT website[11], a new expression for the Maxwellian Average Electron Neutral Cross-section has been proposed and integrated into the plasma models described in this paper.

Calculation of the total pressure within the OHCs has been performed in Ref. 6 and 7. using a modification of Poiseuille flow theory[2] (to take into account compressibility and molecular flow effects) and an equivalent temperature or modified specific gas constant taking into account the ionization fraction[1,4]. Despite of the good results, an analytical description of the flow physics inside the hollow cathode remains a challege. Phenomena not yet properly taken into account concern heat addition from Joule heating in the orifice, frozen flow and wall losses due to ionization and plasma sheath fluxes, a transition from incompressible to sonic flow over the length of a short orifice, viscous effects, and a transition to molecular flow. Recently Taunay *et al.*[12] have proposed an empirical correlation able to calculate the pressure inside OHCs over a range of three orders of magnitude or five orders of magnitude in the non-dimensional space, and able to capture the dependency of the total pressure on the discharge current where theoretical models can not. For this reason, it has been decided to replace the theoretical approach with the empirical one in the model presented in this work.

The resistivity of the internal plasma has been calculated in Ref. 6 and 7 in a similar fashion as in the literature[1,2,3], assuming that current is conducted radially. To account for radial conduction, it was introduced an average cross-sectional area, but a factor of π has been missed in the original expression[8]. An update of the model[6,7] was due in order to take into account this note.

Finally, a model to compute plasma parameters within *keeper region* has been also proposed in order to simulate diode discharge mode of type closed OHCs. Care was taken in the coupling between the orifice and the keeper region. According to Ref. 1, 2 and 13 which follow Andrews and Allen idea[14], the existence of a double-sheath at the entrance of the orifice region is considered. This hypothesis is currently disputed[8]. Goebel *et al.*[15] shows that there is a potential discontinuity in the profiles measured, but it is situated after the orifice entrance and most likely at/after the orifice exit similarly to what Siegfried and Wilbur observed in the keeper region of their cathode in the plume mode[16].

The paper investigates the effect of modeling the double sheath at the orifice exit and at the orifice entrance, studying particularly the differences on the total voltage drop with respect to the discharge current and the mass flow rate.

II. Cathode Architecture

A sketch of a typical Orificed Hollow Cathode configuration is shown Fig. 1(a). A neutral gas (e.g. Xenon, Argon, Krypton) flows in a conductive tube made of refractory metal (e.g. tantalum or molybdenum) or graphite. A low-work function material, namely insert, is placed inside the main tube. The electrons are extracted from the insert material by means of thermionic effect at a lower temperature with respect to the main tube. Several insert materials have been used. The most common are barium-based emitters, equipping the dispenser impregnated cathodes, and rare-earth emitters (e.g. LaB_6, CeB_6), which have respectively a work function of about 2 eV and 2.7 eV. They provide a current densities as high as $10^5 Am^2$ at a surface temperature of about 1300 K and 1900 K, respectively. The first type of emitters are highly susceptible to oxygen contamination while rare-earth based emitters react with many refractory metals at high temperatures (in this case a thin graphite sleeves is placed between the emitter and the main tube).

An orifice plate is placed at the downstream end of the tube to increase the internal pressure. The high pressure results in a low plasma potential, which, in turn, increases the ionization efficiency and reduces the energy of the ions reaching the cathode walls.

The insert reaches the emission temperature with the aid of a heater wrapped around the tube, which is provided with thermal shields to reduce the radiation losses. The cathode tube and heater are surrounded by the keeper electrode, whose function is to help the extraction of the electrons to the discharge plasma and to protect the cathode from the ion bombardment.

III. Model Overview

The model consists of four main modules: the keeper plasma model, the orifice plasma model, the insert plasma model, and the cathode thermal model. The models are consecutively solved by means of an iterative procedure to calculate the plasma properties, along with the temperature profile and heat exchanges in the cathode assembly. The plasma properties are averaged in each control volume, Fig. 1(b), and steady-state conditions are assumed. The quasi-neutral plasma is considered to be a mixture of three perfect gases: thermalized electrons, single-charged positive ions, and neutrals. Ions and neutrals are considered to be at the same temperature of the cathode wall. Cathode's geometry and materials, operative conditions, propellant properties, and the effective emission length are the input of the model.

The main modifications to the model described in Ref. 6, referred here as *Basic* model, are based on the following assumptions:

- Xenon electron-neutral cross section was computed using the formula of Katz *et al.*[9] that fits the total elastic cross section considering the database of Hayashi[20] collected in 1983, instead of the elastic momentum-transfer cross section;
- The plasma resistivity of the internal region was estimated by a formula that missed a π factor;
- The internal pressure was computed using a theoretical approach, that is not able to take into account all the aspect of plasma physics within OHC and did not consider any variation with respect to the discharge current;
- Keeper region plasma parameter were not calculated.

At first a double-sheath at the constriction between the insert and orifice regions will be modelled in agreement with Ref. 1, 2 and 13. Then, the modifications to the equations, need to model the double sheath at the orifice exit section, will be described.

The following subsections will show and discuss the main equations of the model emphasizing the part which have been modified with respect to Ref. 6.

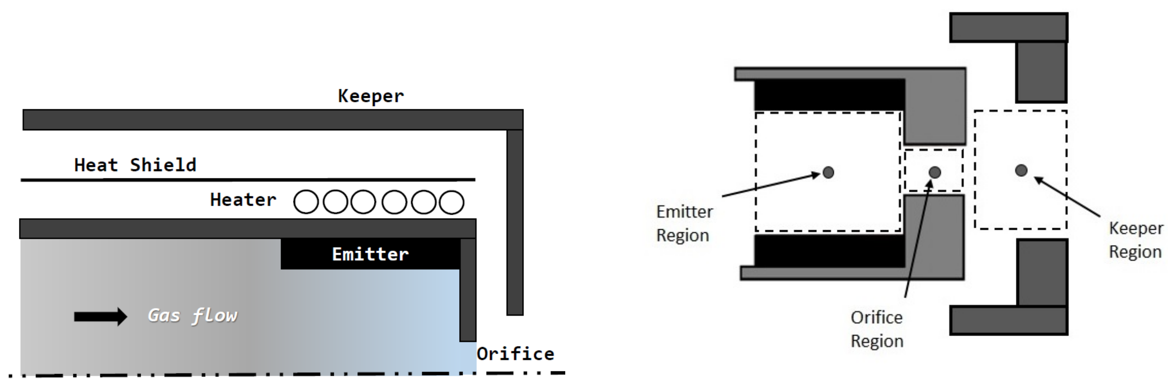

(a) (b)

Figure 1. Architecture of typical Orifice Hollow Cathode (a). Sketch of plasma model regions (b).

A. Double Sheath between orifice and insert regions

1. Keeper Plasma Model

The keeper model is made of three equations expressing current density balance, Eq.1(a), the balance of ion flux, Eq.1(b) and equation of state, Eq.1(c), to compute the plasma number density ($n_{e,k}$), the electron temperature ($T_{e,k}$), and the density of the neutrals ($n_{0,k}$).

$$\begin{cases} \underbrace{n_{e,k} = n_{e,o}\dfrac{A_o}{A_k}\sqrt{\dfrac{T_{e,o}}{T_{e,k}}}}_{j_{i,k}A_k = j_{i,o}A_o} & (a) \\ \underbrace{q\pi r_k^2 L_k n_{0,k} n_{e,k} K_i}_{\dot{n}_{ion,k}} = \underbrace{j_{i,k}\left(2\pi r_k L_k\right) + 2 j_{th,k}\pi r_k^2}_{\dot{n}_{out,k}} & (b) \\ \underbrace{\left(n_{e,k} + n_{0,k}\right) k_B T_{w,k}\left(1 + \dfrac{\alpha T_{e,k}}{T_{w,k}}\right)}_{p_{kin}} = \underbrace{\dfrac{\dot{m}}{\pi r_k^2}\sqrt{\dfrac{R_g T_{w,k}}{\gamma}\left(1 + \dfrac{\alpha T_{e,k}}{T_{w,k}}\right)}}_{p_{cont}} & (c) \end{cases} \quad (1)$$

The first equation, Eq.1(a), states, as a first-order approximation, that plasma density in the keeper region ($n_{e,k}$) scales linearly the orifice plasma density ($n_{e,o}$) with the orifice-to-keeper area ratio (A_o/A_k) and the square root of electron temperatures ratio ($\sqrt{T_{e,o}/T_{e,k}}$), since a remarkable plasma density drop takes place in the orifice-keeper gap[17].

Equation 1(b) writes the balance between the ion production ($\dot{n}_{ion,k}$) and the ion loss rate ($\dot{n}_{out,k}$). A sketch of current density fluxes is depicted in Fig. 2. Ions leave the control volume with the Bohm velocity toward the keeper orifice walls and with the thermal speed upstream to orifice and downstream to the environment (indeed j_i and j_{th} are the Bohm and the thermal current densities, respectively).

The last balance, Eq.1(c), equates the plasma pressure as computed from the kinetic theory of gases (p_{kin}) with the pressure of a continuum (p_{cont}) flow chocked at the orifice exit[1,4].

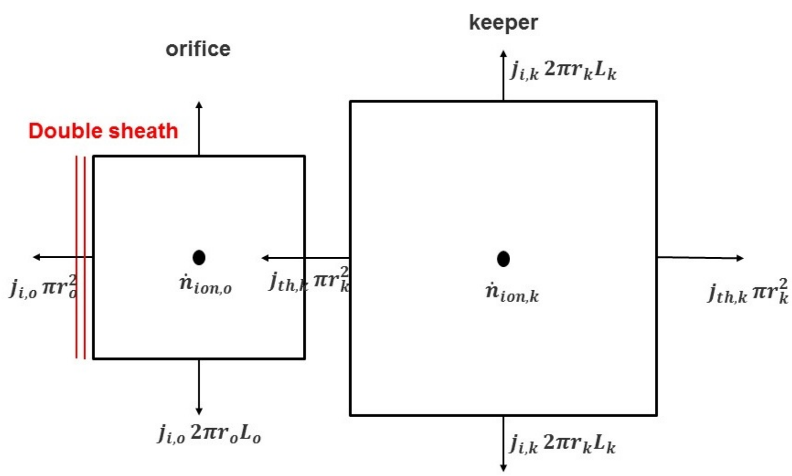

Figure 2. Sketch of ion fluxes when a double sheath is modeled between orifice and emitter regions.

2. Orifice Plasma Model

The system of equations 2 is solved to get the plasma number density ($n_{e,o}$), the electron temperature ($T_{e,o}$), and the density of the neutrals ($n_{0,o}$) in the orifice region.

$$\begin{cases} \underbrace{q\pi r_o^2 L_o n_{0,o} n_{e,o} K_i}_{\dot{n}_{ion,o}} + \underbrace{j_{th,k} A_k}_{\dot{n}_{in,k}} = \underbrace{j_{i,o}\left(2\pi r_o L_o + \pi r_o^2\right) + j_{th,o}\pi r_o^2}_{\dot{n}_{out,o}} & (a) \\ \underbrace{R I_d^2}_{P_{ohm}} = \underbrace{\dot{n}_{ion}\left\langle \epsilon_i \right\rangle}_{P_{ion}} + \underbrace{\frac{5}{2}\frac{k_B}{q} I_d\left(T_{e,o} - T_{e,e}\right)}_{P_{conv}} & (b) \\ \underbrace{\left(n_{e,o} + n_{0,o}\right) k_B T_{wo}\left(1 + \frac{\alpha T_{e,o}}{T_{wo}}\right)}_{p_{kin}} = \underbrace{\frac{\dot{m}}{\pi r_o^2}\sqrt{\frac{R_g T_{wo}}{\gamma}\left(1 + \frac{\alpha T_{e,o}}{T_{wo}}\right)}}_{p_{cont}} & (c) \end{cases} \tag{2}$$

The conservation of the ion flux, Eq.2(a), imposes a balance between the ions formed by ionization ($\dot{n}_{ion,o}$) and the ions crossing the boundaries of the control volume ($\dot{n}_{in,k}$ and $\dot{n}_{out,o}$). Ions moves from keeper to orifice region, Fig.2, since it is expected that the electron temperature increases along the cathode axis[15,18,19]. Equation 2(a) can be rewritten considering the relation between the Bohm and thermal current density ($j_{th} \simeq 0.66 j_i$) and recalling Eq.1(a):

$$q\pi r_o^2 L_o n_{0,o} n_{e,o} K_i = j_i\left[2\pi r_o L_o + \pi r_o^2\left(1 - \frac{1}{4}\frac{1}{0.61}\sqrt{\frac{8}{\pi}}\right)\right] + j_{th,o}\pi r_o^2 \tag{3}$$

This results is very interesting because keeper plasma parameters (densities and temperatures) do not appear. This simplifies the resolution of the full model because no loop from keeper to orifice must be taken into account.

The plasma power balance, Eq.2(b), states that the resistive heating (P_R), balances the energy losses due to neutral-particle ionization (P_{ion}), to the electron convection (P_{conv}), neglecting the ion losses across the double sheath to simplify the coupling with the emitter module. Here the plasma resistance is calculated as:

$$R = \frac{\eta L_o}{\pi r_o^2} \qquad \eta = \frac{\nu m_e}{n q^2} \tag{4}$$

where η is the plasma resistivity that depends on the total collision frequency which includes the contributions of electron-ion and electron-neutral collisions ($\nu = \nu_{ei} + \nu_{en}$). Particularly the electron-neutral collision is proportional to the Maxwellian Average Cross section, $\langle\sigma_{en}\rangle$:

$$v_{en} = \langle\sigma_{en}\rangle\, n_0\left(\frac{k_B T_e}{n_e}\right) \tag{5}$$

According to literature[1,2,3,13], the Basic model[6] used the numerical correlation[9] of Katz *et al.* which fits old data of total collision cross-section of Xenon[20], which also includes inelastic collisions, instead of the momentum transfer cross-section[8]. The present model, on the other hand, features a new correlation for the most recent elastic electron-neutral cross section[11]. The fit agrees with experimental data with an R-squared value of 0.99 and it works in the range of electron temperature 0.1÷10eV and gives cross section values in square meters, Eq. 6.

$$Log_{10}(\langle\sigma_{en}\rangle) = \frac{p_1 {T_e^*}^5 + p_2 {T_e^*}^4 + p_3 {T_e^*}^3 + p_4 {T_e^*}^2 + p_5 T_e^* + p_6}{{T_e^*}^2 + q_1 T_e^* + q_2}, T_e^* = Log_{10}(T_{eV}) \tag{6}$$

	p_1	p_2	p_3	p_4	p_5	p_6	q_1	q_2
Values	0.0350	−0.3057	−0.6698	−18.5416	−12.8821	−9.9614	0.7093	0.5227

The last equation of system 2 equates the pressure computed by the kinetic theory of gases (p_{kin}) with the pressure of continuum flow (p_{cont}), just like modelled in the keeper region (Eq. 1(c)).

3. Insert Plasma Model

The insert plasma model is composed of four equations. The unknown are the plasma number density ($n_{e,e}$), the electron temperature ($T_{e,e}$), the density of the neutrals ($n_{0,e}$) and the emitter sheath voltage drop (V_p) in the insert region.

$$
\begin{cases}
\underbrace{q\pi r_e^2 L_{eff} n_{0,e} n_{e,e} K_i}_{\dot{n}_{ion,e}} + \underbrace{j_{i,o}\pi r_o^2}_{\dot{n}_{in,o}} = \underbrace{j_{i,e}\left(A_{eff} + \pi r_e^2 - \pi r_o^2\right) + j_{th,e}\pi r_e^2}_{\dot{n}_{out,e}} & (a) \\
j = \frac{I_d}{A_{eff}} = j_{i,e} + j_{em} - j_{er} & (b) \\
\underbrace{j_{i,o}\left(V_{ds} + 2\frac{k_B T_s}{q}\right)\pi r_o^2}_{P_{i,o}} + \underbrace{R I_d^2}_{P_{ohm}} + \underbrace{j_{em}\left(V_p + \frac{3}{2}\frac{k_B T_s}{q}\right)A_{eff}}_{P_{em}} = & \\
\underbrace{\dot{n}_{out,e}\left(\langle\varepsilon_i\rangle + 2\frac{k_B T_s}{q}\right)}_{P_i} + \underbrace{j_{er} 2\frac{k_B T_s}{q} A_{eff}}_{P_{er}} + \underbrace{\frac{5}{2}\frac{k_B T_{e,e}}{q} I_d}_{P_{conv}} & (c) \\
\underbrace{\left(n_{e,e} + n_{0,e}\right) k_B T_s \left(1 + \frac{\alpha T_{e,e}}{T_s}\right)}_{p_{kin}} = \underbrace{1.36 \cdot 10^{-9} \frac{{I_d}^{0.3} {T_g}^{0.95} \dot{m}^{0.57} {L_o}^{0.15}}{M^{0.10} {\epsilon_i}^{0.20} \mu^{0.35} {d_e}^{1.43} {d_o}^{1.71}}}_{p_{emp-corr}} & (d)
\end{cases}
\tag{7}
$$

The ion balance, Eq.7(a), has been written equating the sum of ion production rate due to direct electron-impact ionization ($\dot{n}_{ion,e}$) and the contribution of the ions generated in the orifice with accelerated toward the insert as they cross the double sheath ($\dot{n}_{in,o}$) with the losses at the sheath boundaries as well as the thermal flux to the upstream section of the control volume ($\dot{n}_{out,e}$).

In the current conservation equation, Eq.7(b), the total current is the sum of the ion current density collected at the emitter surface, as computed from the Bohm sheath criterion (j_i) the thermionic current density (j_{em}) minus the thermal flux of electrons recombining on the insert wall (j_{er}).

The power balance at the plasma, Eq.7(c), takes into account the plasma heating due to the Joule effect (P_{ohm}), the energy delivered to the plasma by the ions of the orifice, ($P_{i,o}$), as well as the energy gain due to the emitted electrons (P_{em}). The energy is lost by the ions leaving the control volume (P_i), and the electrons recombining on the emitter surface (P_{er}), as well as by the effect of the electron current convection, (P_{conv}). Here the formula for the calculation of plasma resistance has been corrected with respect to the Basic model[6] adding a π to the denominator[8], Eq. 8.

$$R = \frac{3\eta}{4\pi L_{eff}} \tag{8}$$

The model assumes the existence of a planar double sheath at the entrance of orifice[1,2,13]. The value of voltage drops is computed by means of the formula of Capacci *et al.*[13] who simplifies the rigorous derivation of a double-sheath potential over a distance d described by Langmuir[21].

$$V_{ds} = \left(\frac{9 I_d k_B T_{e,o}}{7.5\pi n_{e,o} r_o^2 q^2}\sqrt{\frac{m_e}{2q}}\right)^{2/3} \tag{9}$$

Particularly, Capacci *et al.*[13] consider the distance between the two planar sources of charged species as the Debye length (λ_D) computed using orifice plasma electron density and temperature.

In this work it is preferred an empirical approach to calculate the total static pressure inside the OHCs over the theoretical one[1] implemented in the Basic model[6]. The selected empirical correlation[12], RHS of Eq.7(d), agrees with the fitted experimental data with an R-squared value of 0.98 and average error of 24.5%, and allows to capture the dependency of the pressure with both mass flow rate and discharge current, while theoretical models can not. Moreover the cathode internal pressure can be computed over an extremely wide range of operating conditions that could not be captured by a flow model incorporating only a single flow regime.

According to the empirical correlation, pressure in the insert region in Pa is a function of the orifice and insert diameters (d_o, d_e) in meters, the orifice length (Lo) in meters, the discharge current (I_d) in Amperes, the mass flow rate ($\dot{m}$) in kg/s, the atomic mass of the propellant considered (M) in kg, the ionization energy of the species considered (ϵ_i) in eV, the dynamic viscosity (μ,) in Pa·s and the gas temperature (T_g) in K.

4. Thermal Model

A Lumped Elements Thermal Model, named LETherM[7], has been developed to quickly compute the temperature profile along the cathode axis, and more particularly the insert and orifice temperatures (used in the plasma model). The cathode is subdivided into few elements with the purpose of getting a simple thermal network, where each node refers to a specific element. Perfect contact conditions are assumed among the cathode elements and the thermal deformations are neglected thus considering constant areas for heat exchanges. The thermal model includes temperature dependent expressions for the thermal conductivity of the materials and for the surfaces' emissivity[7]. The model allows to assign different material properties for each node.

The temperatures of the nodes are obtained by solving the set of equations having fixed a cathode base temperature that have been varied in the range 800-1200 K. Two types of equation compose the system depending on the type of node. The first power balance writes:

$$-P_{in} + \frac{\left(\sigma_{SB} T_i^4 - J_i\right)}{R_i} + \frac{\sum_j \left(T_i - T_j\right)}{R_{cond_{i,j}}} = 0 \tag{10}$$

where, σ_{SB} is the Stefan-Boltzmann constant, R, are the equivalent resistance and P_{in} stands for the external power input to node i-th. Particularly the emitter is heated by the ions recombining on the wall and the back-streaming electrons, while is cooled by the emitted thermionic electrons leaving the surface whereas the ohmic power, as computed in the orifice model, is assumed to be completely transferred to the orifice wall. The power balance of the node representing the insert includes the loss by evaporation, too. The convective heat transfer is included in the model where nodes are in contact with gas.

For the second kind of node the power balance is expressed as:

$$\sum_j \frac{\left(J_i - J_j\right)}{R_{i,j}} - \frac{\left(\sigma_{SB} T_i^4 - J_i\right)}{R_i} = 0 \tag{11}$$

The background temperature for radiation has been set to 300 K.

Keeper nodes are not modelled. Keeper wall temperature has been supposed to be a constant fraction of orifice wall temperature. According to the experimental measurements provided in literature[22] and FEM simulations, a keeper-to-orifice wall temperature ratio of 0.8 has been used.

B. Double Sheath between orifice and keeper regions

The modifications of the plasma models' equations, required to account for the double sheath between orifice and keeper regions, will be presented in the following subsections. The sketch of ions current density fluxes in this case is depicted in Fig.3. Modifications of the thermal model were not needed.

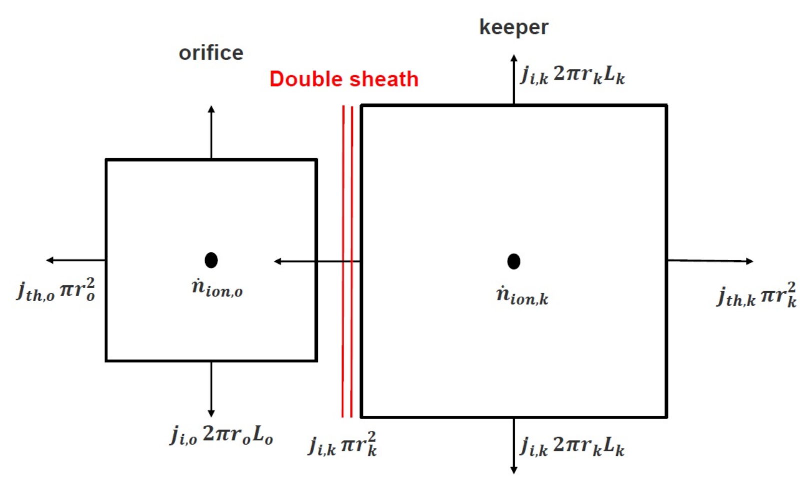

Figure 3. Sketch of ion fluxes when a double sheath is modeled between orifice and keeper regions.

1. *Keeper Plasma Model*

The ion balance equation, Eq.1(b), was modified considering the flux of ions through the double sheath ($j_{i,k}$), that is calculated by means of the Bohm condition.

$$q\pi r_k^2 L_k n_{0,k} n_{e,k} K_i = j_{i,k}\left(2\pi r_k L_k + \pi r_k^2\right) + j_{th,k}\pi r_k^2 \tag{12}$$

2. *Orifice Plasma Model*

To take into account that ions move counter-streaming from keeper region to orifice with Bohm velocity, the therm $\dot{n}_{in,k}$ of Eq. 2(a) was updated.

$$q\pi r_o^2 L_o n_{0,o} n_{e,o} K_i + \underbrace{j_{i,k} A_k}_{\dot{n}_{in,k}} = j_{i,o}\left(2\pi r_o L_o + \pi r_o^2\right) + j_{th,o}\pi r_o^2 \tag{13}$$

The equation can be rewritten considering Eq.1(a) as follows:

$$q\pi r_o^2 L_o n_{0,o} n_{e,o} K_i = j_{i,o}\left(2\pi r_o L_o\right) + j_{th,o}\pi r_o^2 \tag{14}$$

3. *Insert Plasma Model*

The contribution due to the incoming ions from the orifice ($\dot{n}_{in,o}$) in the ion balance Equation 7(a) was updated because ions enter in emitter region with thermal speed (Eq. 15). The energy delivered to the plasma by the ions of the orifice ($P_{i,o}$) in the power balance equation, Eq.7(c), was modified for this reason and to account for the displacement of the double sheath , Eq. 16.

$$q\pi r_e^2 L_{eff} n_{0,e} n_{e,e} K_i + \underbrace{j_{th,o}\pi r_o^2}_{\dot{n}_{in,o}} = j_{i,e}\left(A_{eff} + \pi r_e^2 - \pi r_o^2\right) + j_{th}\pi r_e^2 \tag{15}$$

$$\begin{aligned} &\underbrace{j_{th,o}\left(2\frac{k_B T_s}{q}\right)\pi r_o^2}_{P_{i,o}} + R I_d^2 + j_{em}\left(V_p + 2\frac{k_B T_s}{q}\right) A_{eff} = \\ &\dot{n}_{out}\left(\langle\varepsilon_i\rangle + 2\frac{k_B T_s}{q}\right) + j_{er} 2\frac{k_B T_s}{q} A_{eff} + \frac{5}{2}\frac{k_B T_e}{q} I_d \end{aligned} \tag{16}$$

IV. Results

The results of the models are presented in the following sections, along with a preliminary validation of the models themselves. The baseline cathode geometry is that of ALPHcA developed and tested by SITAEL[23,24]. It consists of a tantalum tube 7.5 mm in diameter, with a polycrystalline LaB6 insert 3 mm in internal diameter and 6 mm in length. Given the reactivity of LaB6 with refractory metals at high temperature, the direct contact between the emitter and the tube is prevented by means of thin graphite sleeves in a cup-arrangement at the insert ends. The thickness and the length of the tube are approximately equal to 0.3 mm and 20.6 mm, respectively. The orifice has a diameter of 0.4 mm and a length of 0.36 mm. The molybdenum-alloy keeper presents a 0.6 mm diameter orifice, whereas the cathode-to-keeper gap is 2 mm in the longitudinal direction. Because the length of keeper orifice has not been found, a realistic value of 0.3 mm has been selected to perform the calculation. The propellant is pure Xenon (contamination issues are not considered in the model). The cathode operates at a discharge current ranging from 1 to 3 A and at mass flow rates between 0.08 and 1 mg/s. In this operational envelope, electrical characteristics in diode mode with keeper, are reported in Ref. 24.

A. Mass Flow Rate sensitivity study

The effect of the mass flow rate on the plasma parameters is presented for ALPHcA at a discharge current of 3 A. At first the effect of model updates will be shown; then the effect of the position of double sheath (before orifice entrance and after the orifice exit) will be discussed.

1. Effect of Model updates

The average plasma densities and electron temperatures in the insert and the orifice regions are reported in Fig. 4 as a function of mass flow rate for ALPHcA operating at 3A of discharge current. The comparison between the numerical results of the basic model and the updated one is presented. The plasma densities increase with mass flow rate consistently with both theoretical and experimental trends found in the literature[4,25] The electron temperature plots in the two cathode regions display a decreasing trend as in Ref. 2, 4 and 25. Both emitter and orifice surface temperature (Fig. 5) increases with mass flow rate, according to Ref. 22 and 25.

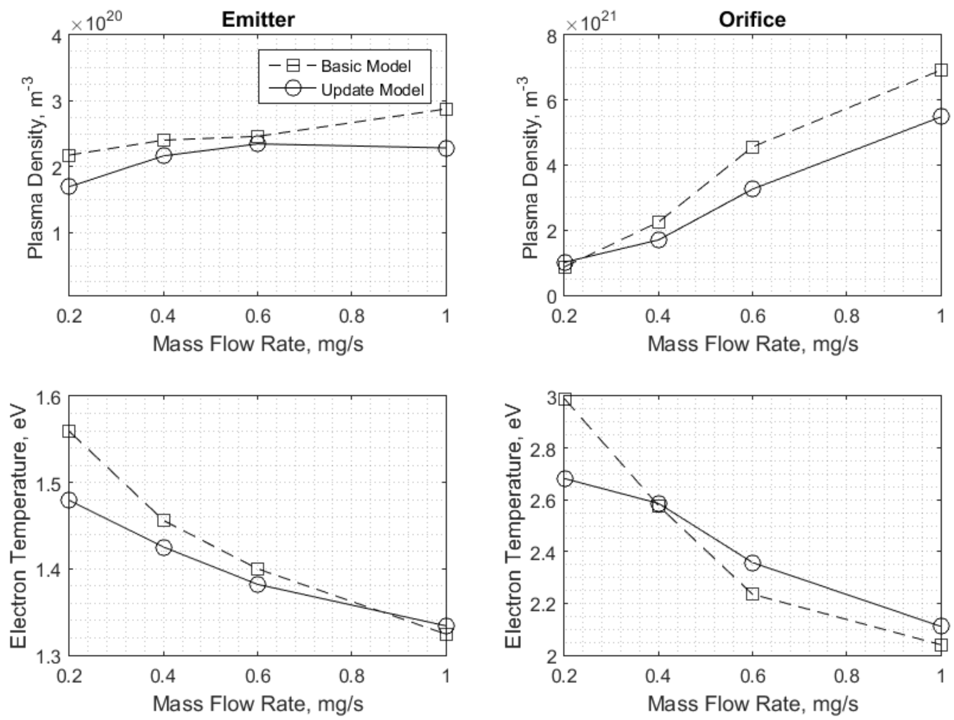

Figure 4. Plasma densities and electron temperatures in the insert and the orifice regions as function of mass flow rate for ALPHcA at 3A: Numerical Results.

The plot of the effective emission lengths as function of mass flow rate are reported in Fig. 6 at 3 A. The results of the update model particularly show a decreasing trend as theoretically[25] and experimentally[26] verified in literature.

The dependence of the discharge voltage on the mass flow rate for ALPHcA is shown in Figure 7 for a discharge current of 3 A. The numerical value of total voltage, V_t, is computed by the basic model as the sum of the potential drops from the emitter to the orifice:

$$V_t = V_e + V_p + V_{ds} + V_o \tag{17}$$

where V_e and V_o are the ohmic potential drops in the emitter and orifice regions, respectively, V_{ds} is the voltage drop between emitter and orifice regions and V_p is the emitter sheath voltage drop. Because the keeper plasma region a new ohmic contribution, V_k, must be added to the Eq. 17:

$$V_t = V_e + V_p + V_{ds} + V_o + V_k \tag{18}$$

The discharge voltage displays the typical increase at the lowest values of mass flow rate (plume mode) and both models predict values of tension on average ± 1 to 3% the experimental value, Fig. 7.

Figure 8 reports the distribution of plasma density, electron temperature and pressure along the ALPHcA cathode axis at 3 A and 1 mg/s computed by means of the updated model. The trend of a linearly increasing plasma electron temperature and increasing-decreasing plasma density along the cathode axis is evident from

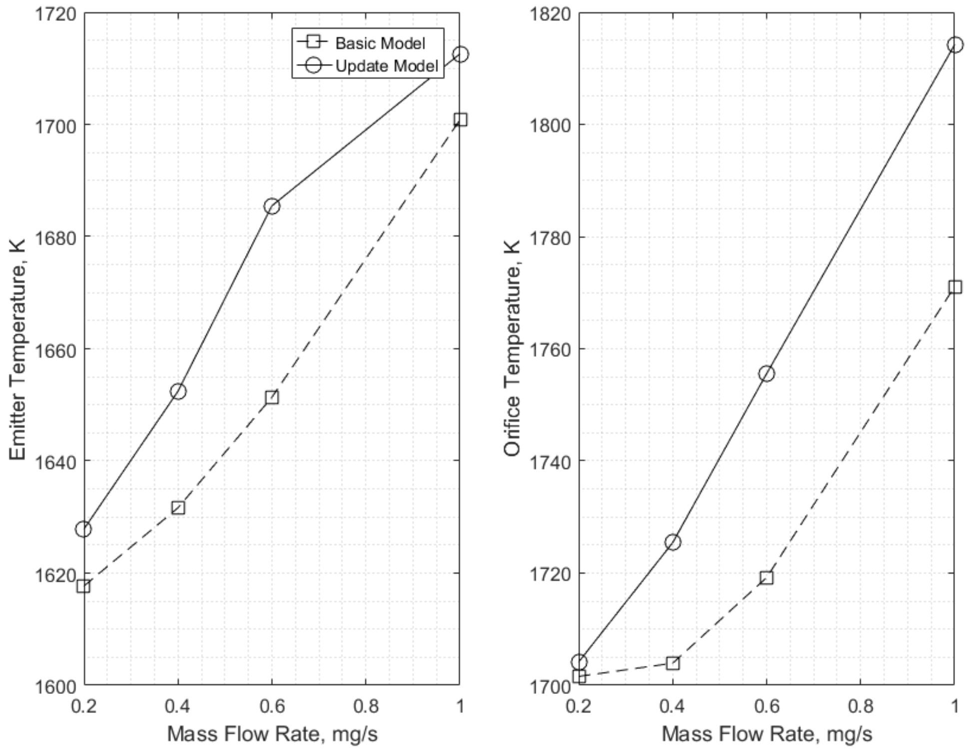

Figure 5. Emitter and the orifice wall temperatures as function of mass flow rate for ALPHcA at 3A: Numerical Results.

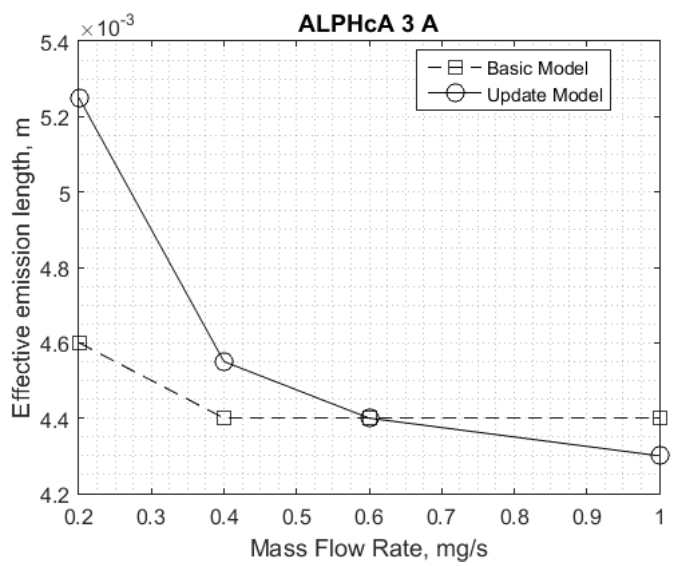

Figure 6. Effective emission length as a function of mass flow rate for ALPHcA at 3 A. Numerical result.

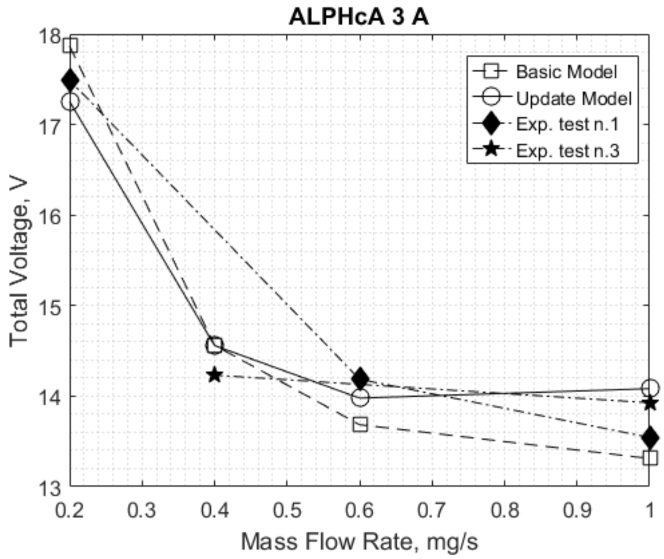

Figure 7. Discharge voltage as function of the mass flow rate for ALPHcA at 3A: Numerical results vs. experimental data (Test n.1 and n.3 from Ref. 24)

the experiments performed by several authors[18,22,26] and is correctly predicted by the model, Fig. 8(a). Moreover, as expected, pressure decreases along the cathode axis, Fig. 8(b).

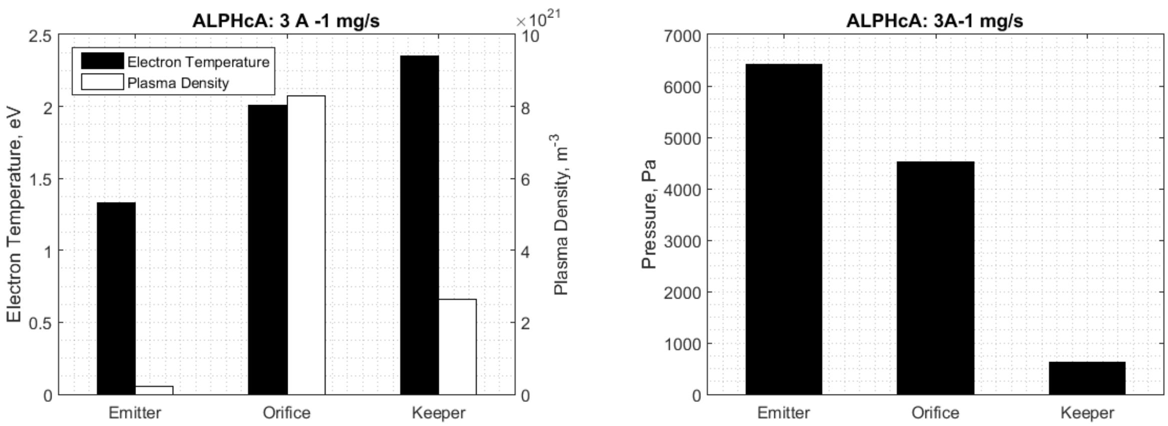

(a)

(b)

Figure 8. Distribution of plasma density, electron temperature and pressure along the ALPHcA cathode axis at 3 A and 1 mg/s. Numerical results.

The dependence of the internal pressure on mass flow rate for ALPHcA is shown in Fig.9. Particularly, the comparison between the Basic and the update model is reported in Fig.9(a), whereas Fig.9(b) compares the internal pressure, computed with the update model, with the experimental data at 1.5A. It is worth to notice that the grow rate of pressure with the mass flow rate is under predicted with respect to the experimental data because the insert plasma model features the assumption that the temperature of heavy species (ions and neutrals) is set equal to the wall temperature.

2. Effect of the position of the Double Sheath

The effect of modeling the double sheath at the orifice exit on the total voltage is studied here for ALPHcA, setting a discharge current of 3A. Figure 10 reports the total discharge voltage plots computed considering the Double Sheath (DS) at orifice entrance and at orifice exit. It is interesting to note that with the

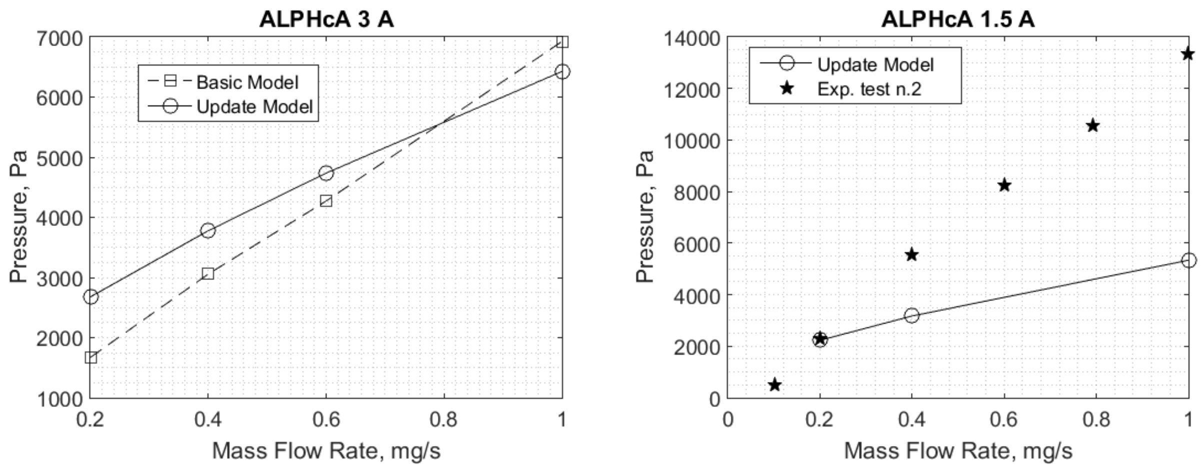

(a) Numerical results (b) Numerical results vs experimental data[24]

Figure 9. Internal pressure as a function of mass flow rate for ALPHcA at 3 and 1.5 A.

second assumption the model predicts with good approximation the tension values in plume mode but it underestimates them in spot mode, with an increasing trend with respect to mass flow rate.

The total discharge voltages have been computed using Eq. 18. Care was taken evaluating the double sheath voltage drop intensity (V_{ds}). The formula of Capacci *et al.*[13] refers to a Debye length computed with the plasma density and the electron temperature of the orifice region, when the double sheath is modeled at the orifice entrance. To verify if this assumption would be still suitable when the double sheath is modeled at the orifice exit, two experimental test campaigns, where the plasma potential profile along the axis were measured, have been selected. The cathodes tested are the NSTAR[15,18,19] and the Sigfried and Wilbur[27] Hg cathode. The double sheath voltage drops (V_{ds}) have been computed using both orifice and keeper plasma parameters and they have been compared to the retrieved experimental values in Table 2.

For both the NSTAR operation levels considered (namely TH15 and TH8), the best agreement with the experimental value is obtained using the keeper plasma parameters. Here it has been verified experimentally that a large voltage drop occurs after the orifice exit[15,18,19].

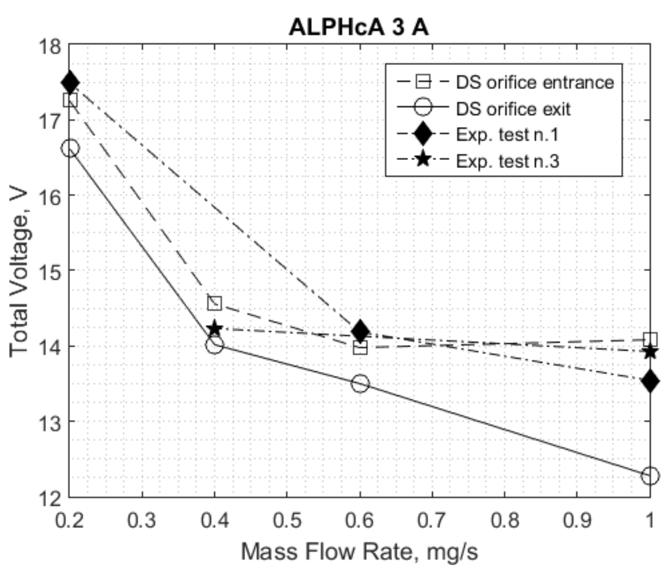

Figure 10. Discharge voltage as function of the mass flow rate for ALPHcA at 3A: Numerical results vs. experimental data (Test n.1 and 3 from Ref 24) .

Sigfried and Wilbur[27] reports the plasma potential profile both in plume and spot mode, where a potential drop is located, respectively, at the orifice entrance and at the orifice exit. In the first case the intensity of voltage drop (V_{ds}) closest to the experimental value is computed using keeper plasma parameter. On the contrary, in the second one, where the double sheath is located near the orifice entrance, the best result is obtained using orifice parameters.

As a result, the intensity of a double sheath located after the orifice exit has been calculated using keeper plasma parameter in the formula of Capacci *et al.*[13] (Eq. 9).

CATHODE	**NSTAR[15,18,19]**		**Hg Cathode[27]**	
	(TH 15)	**(TH 8)**		
mode	spot	spot	plume	spot
I_d, A	13.3	8.24	2	6
d_o, mm	1.02	1.02	0.75	0.75
$n_{e,o}$, m^{-3}	4.70E+20	3.60E+20	1.00E+20	3.00E+19
$T_{e,o}$, eV	1.4	1.4	0.5	0.5
$n_{e,k}$, m^{-3}	2.30E+19	5.00E+19	1.00E+18	3.00E+18
$T_{e,k}$, eV	2.0	2.0	0.5	0.5
V_{ds} (location)	after orif.exit	after orif.exit	after orif.exit	before orif.entrance
V_{ds}, V	**6**	**4**	**6**	**2**
V_{ds}, V (Orifice*)	**0.72**	**0.63**	**0.43**	**2.02**
V_{ds}, V (Keeper†)	**6.85**	**3.16**	**9.36**	**9.36**

Table 1. NSTAR/Hg cathodes test cases. Comparison of the Double Sheath Voltage Drop, V_{ds}, computed using orifice plasma parameter (*) and keeper plasma parameter (†), with the experimental value.

B. Discharge current sensitivity study

This section reports the electrical characteristics and plasma parameters of ALPHcA at low, 0.2 mg/s, and high, 1 mg/s, mass flow rate as function of the discharge current.

The average plasma densities and electron temperatures in the insert and the orifice regions are reported in Fig. 11 as a function of discharge current at 0.2 mg/s Xe mass flow rate. Figure 11 shows the results of both models with DS at the orifice entrance and after the orifice exit. The dependence of the plasma densities on discharge current is consistent with both theoretical and experimental trends found in the literature[4,25,28]. The electron temperatures in this two cathode regions display a decreasing trend[4] even if that of insert is negligible dependent on the considered range of discharge current as shown in Ref. 17. Little gap between the models' predictions is visible on plasma density and electron temperature in the orifice region. The difference between the results depends on the velocity with which ions come from keeper region, i.e. Bohm or thermal speed.

Plasma density and electron temperature as function of discharge current in keeper region, Fig. 12, show an increase trend in accordance to literature[17,27].

Emitter and orifice wall temperatures as function of discharge current are reported in Fig. 13. Temperatures increase with discharge current, consistently with both theoretical and experimental trends found in the literature[4,25,27]. The internal pressure increases with the discharge current at 0.2 mg/s, Fig. 14, as expected by the empirical correlation, RHS of Eq. 7(d). The results obtained by the models are almost overlapped. The basic model, using the theoretical model to compute the internal pressure, does not predict the dependence on the discharge current.

Total voltage as function of discharge current at 0.2 mg/s Xe mass flow rate is shown in Fig. 15. Numerical data computed by the model with the double sheath at the orifice exit, are, on average, 8% below the experimental Test 1 from Ref. 24. It is interesting to observe that the total voltage are close to those obtained modeling the double sheath between the orifice and the emitter. An exception it is found at 1.5 A where the model with a DS at the orifice entrance underpredict of 20% the experimental data.

The experimental data presented in Ref. 24, show that when the mass flow rate is 0.2 mg/s the cathode

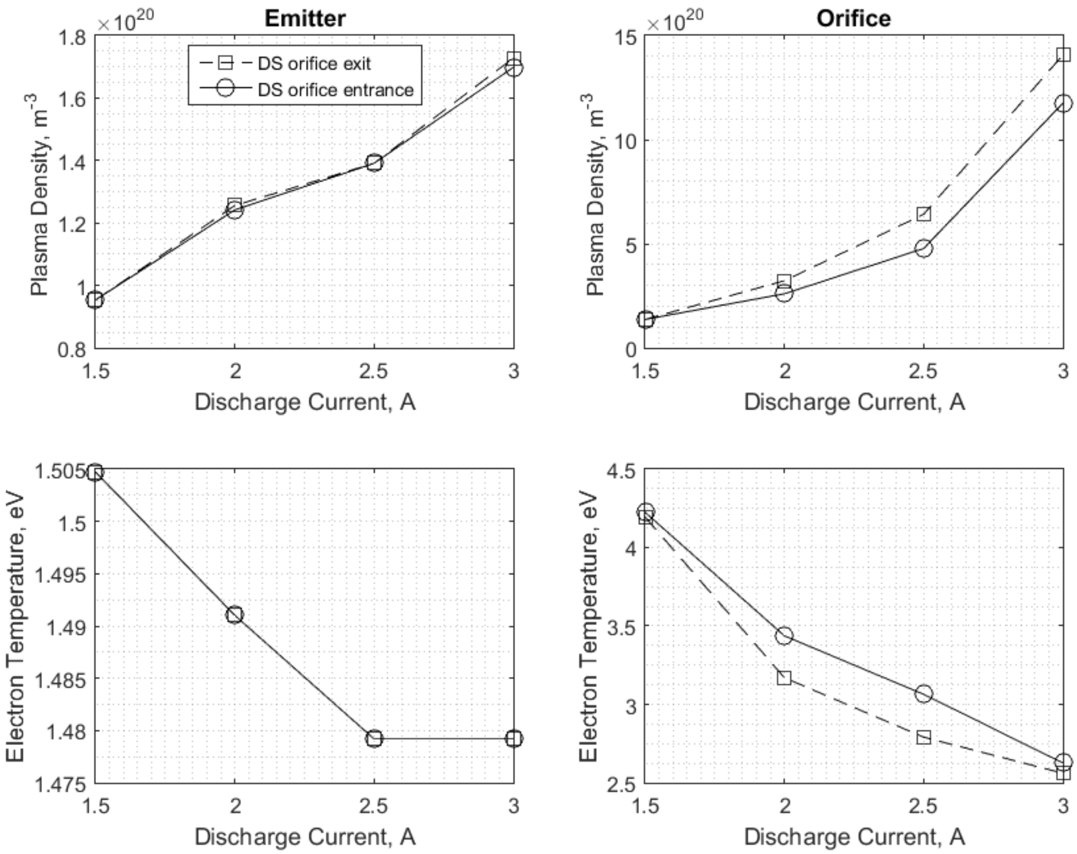

Figure 11. Plasma densities and electron temperatures in the insert and the orifice regions as function of discharge current for ALPHcA at 0.2mg/s: Numerical Results.

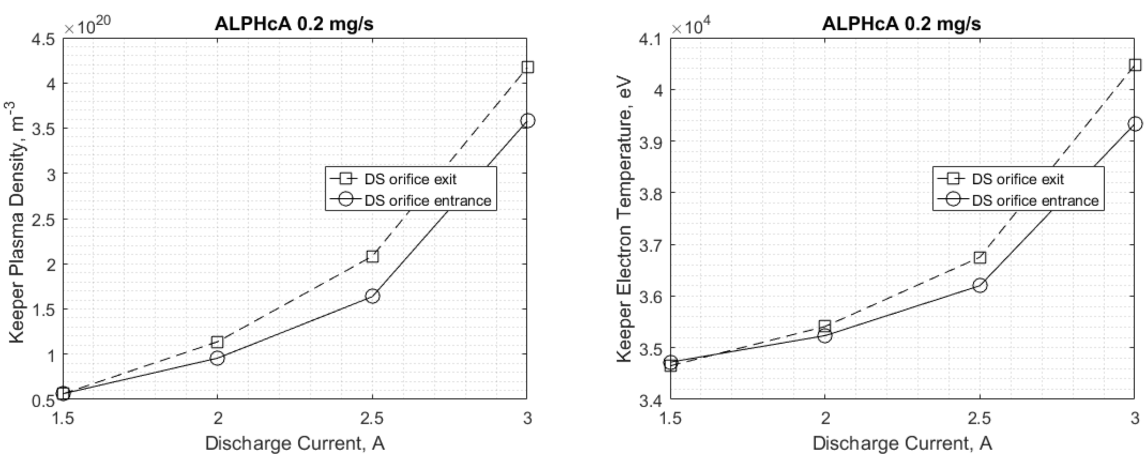

(a)

(b)

Figure 12. Plasma densities and electron temperatures in the keeper region as function of discharge current for ALPHcA at 0.2mg/s: Numerical Results.

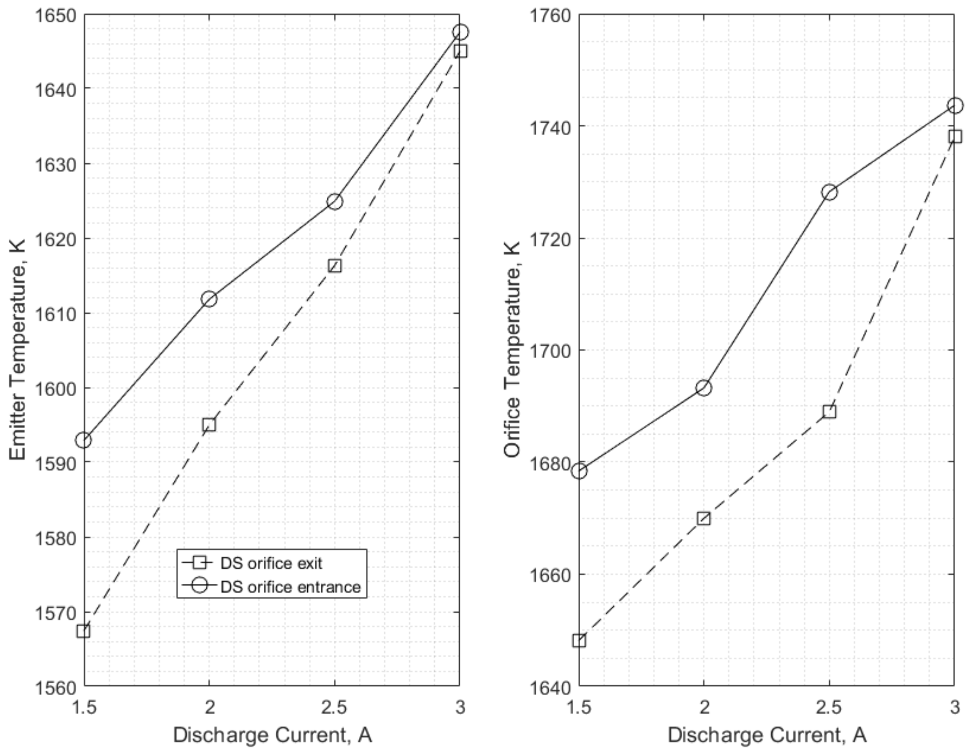

Figure 13. Emitter and the orifice wall temperatures as function of discharge current for ALPHcA at 0.2mg/s: Numerical Results.

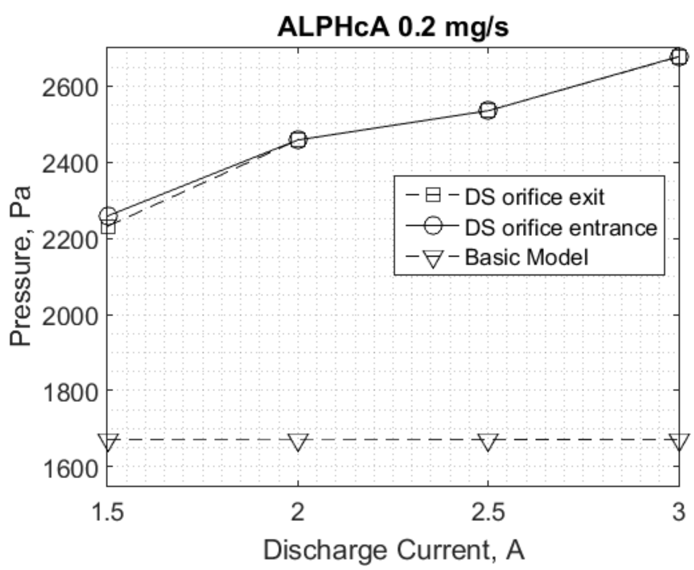

Figure 14. Internal Pressure as function of the discharge current for ALPHcA at 0.2mg/s: Numerical Results.

operates in plume mode for every discharge current. In accordance with the results discussed above (cf. section A.2) it seems that the code modeling the double sheath at the orifice exit, for this type of cathode, works well in plume mode, when a large voltage drop occurs.

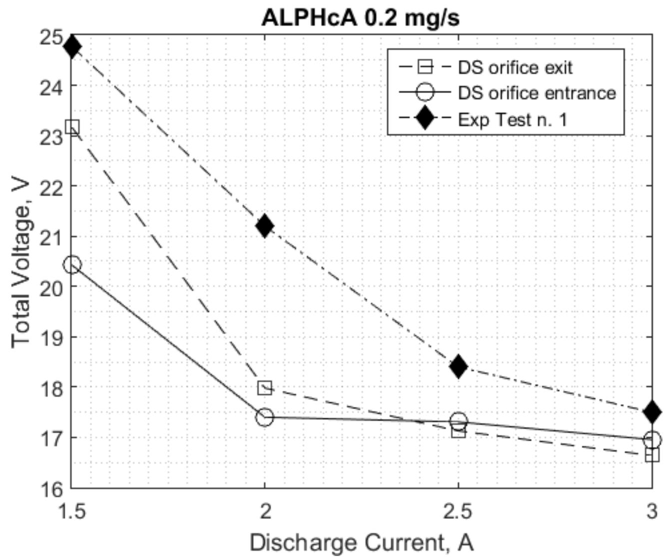

Figure 15. Discharge voltage as function of the discharge current for ALPHcA at 0.2mg/s: Numerical results vs. experimental data (Test 1 from Ref. 24).

Finally Figure 16 reports the total voltage as function of discharge current at 1 mg/s computed with the aid of the numerical code modeling the double sheath at orifice entrance compared to the experiment. Numerical data are presented collecting all the solutions obtained varying the effective emission length (L_{eff}), that is an input parameter of the model. The experimental electrical characteristics are plotted, having gathered all the available data from the test campaign performed by Albertoni *et al.*[24]. The model produces very good agreement with the experiment.

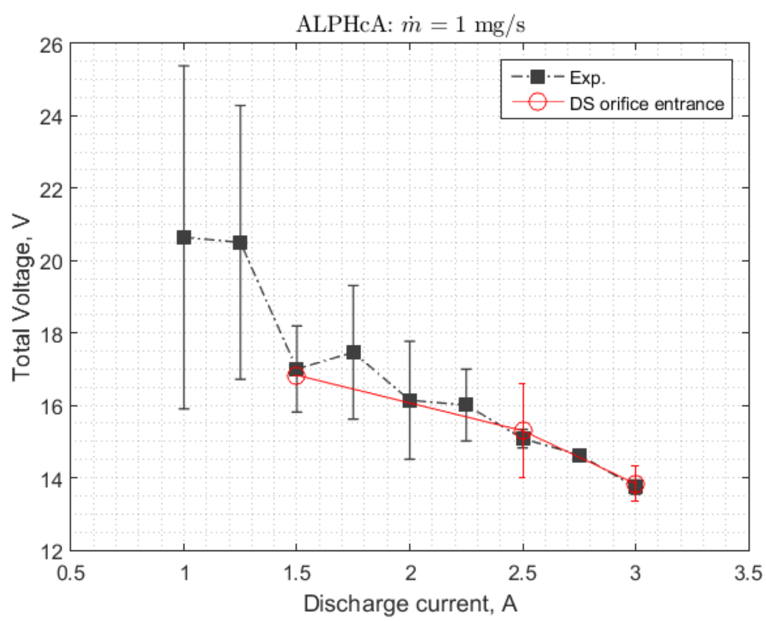

Figure 16. Total voltage as function of discharge current for ALPHcA at 1 mg/s: Numerical Results vs. experiments[24].

V. Conclusion

The updates of the zero-dimensional plasma model for Orificed Hollow Cathodes developed at the Italian Aerospace Research Centre have been presented. An empirical approach have been used to compute the internal pressure. The calculation of the internal plasma resistance has been reviewed. A new fit formula of the most recent experimental data of Xenon elastic collision cross section has been proposed. Furthermore, a keeper plasma region has been included.

The model has been applied to a LaB6 based cathode. The updated model is still able to predict both the trends of the plasma parameters and wall temperatures with mass flow rate and discharge current, as found in literature. Particularly the empirical approach for the calculation of the internal pressure allows to predict also its variations with the discharge current.

The total voltage drop as function of mass flow rate when cathode is operating at 3A has been rebuilt with an accuracy ranging from 1 to 6%. The electrical characteristic at 0.2mg/s have been also studied. It was found that the numerical results under-predict the total voltage on average by 8%.

The variation of the internal pressure with the mass flow rate at 1.5A has been studied. The model is able to predict that pressure increases but the gap between the numerical results and the experimental values grows, too. These outcomes suggest a critical review and a refinement of the model, particularly regarding the calculation of heavy species temperatures.

Finally, the paper has investigated the effect of modeling a double sheath after the orifice exit. According to the study the total discharge voltages are predicted with 1÷5% of approximations in plume mode but the model tends to underestimate tensions in spot mode. Here the difference between the numerical and the experimental data increases with respect to the mass flow rate.

Acknowledgments

The authors would like to thank the italian istitutions which enthrust the realization of PRORA (Programma Operativo Ricerche Aerospaziali) to the Italian Arospace Research Center S.c.p.a. (CIRA) who decided, together the partners (Agenzia Spaziale Italiana, ASI, regione Campania and Ministero dell'Istruzione dell'Universita' e della Ricerca, MIUR) to allocate part of the PRORA funds on the implementation of the Electric Propulsion Program, called IMP-EP. The authors would like to thank also all people involved in the IMP-EP project.

References

[1]Albertoni, R., Pedrini, D., Paganucci, F. and Andrenucci, M., "A reduced-order model for Thermionic hollow cathodes", *IEEE Trans. Plasma Sci.*, vol. 41, no. 7, 2013, pp. 1731-1745.

[2]Domonkos, M. T., "Evaluation of low current orificed hollow cathode", Ph.D. Dissertation, Dept. Aerosp. Eng., Univ. Michigan, Ann Arbor, MI, USA, 1999.

[3]Korkmaz, O., "Global numerical model for the evaluation of the geometry and operation condition effects on hollow cathode insert and orifice region plasmas", MSc Dissertation, Bogazici Univ., 2015.

[4]Salhi, A., "Theoretical and experimental studies of orificed, hollow cathode operation", Ph.D. Dissertation, Ohio State Univ., 1993.

[5]Invigorito, M., Ricci, D., Battista, F., Smoraldi, A., Panelli, M., Salvatore, V., "Activities On Electric Space Propulsion At Italian Aerospace Research Centre: Main Achievements And Outlook", *Proceedings of* 6^{th} *ESA Space Propulsion Conference, SPC2016*, Seville, SP, 14-18 May 2018.

[6]Panelli, M., Smoraldi, A., Battista, F., "A Preliminary Design Tool for Hollow Cathodes", *Proceedings of* 35^{th} *Int. Electric Prop. Conf., IEPC2017*, Georgia Institute of Technology, Atlanta, Georgia, USA, October 8-12, 2017.

[7]Panelli, M., Smoraldi, A., De Simone, V., Battista, F., "Development and Validation of Simplified 1D Models for Hollow Cathode Analysis and Design", *Aerotecnica Missili e Spazio*, Journal of Aerospace and Science Technology, Vol. 97, n. 2, 2018.

[8]Wordingham, C. J., Taunay, P.Y. and Choueiri, E. ,"A Critical Review of Orificed Hollow Cathode Modeling", *Proceedings of* 53^{rd} *AIAA/SAE/ASEE Joint Propulsion Conference*, Atlanta, GA, July 10-12, 2017.

[9]Katz, I., Mandell, J., Patterson, M., Domonkos, M., "Sensitivity of Hollow Cathode Performance to

Design and Operating Parameters", *Proceedings of* 35^{th} *AIAA /ASME /SAE /ASEE Joint Propulsion Conf. Exhibit*, Los Angeles, CA, USA, June 20 -23, 1999.

[10]Hayashi, M., "Bibliography of Electron Photon Cross Sections with Atoms and Molecules Published in the 20th Century - Xenon", National Institute for Fusion Science, NIFS-DATA-79, 2003.

[11]LXCAT website: https://fr.lxcat.net/home/

[12]Taunay, P. C. R., Wordingham, C. J. and Choueiri, E. "An empirical scaling relationship for the total pressure in hollow cathodes", *AIAA Propulsion and Energy Forum"*, Cincinnati, OH, July 2018.

[13]Capacci, M., Minucci, M., and Severi, A., "Simple numerical model describing discharge parameters in orificed hollow cathode devices", *Proceedings of* 33^{rd} *Joint Prop. Conf. and Exhibit*, Seattle, WA, U.S.A., 6 - 9 July 1997.

[14]Andrews, J. G. and Allen, J. E. Theory of a Double Sheath between Two Plasmas" *Proc. R. Soc. Lond. A*, 1971, 320, pp.459-472.

[15]Goebel, D. M., Jameson, K. K., Watkins, R. M., Katz, I. and Mikellides, I. G., "Hollow cathode theory and experiment. I. Plasma characterization using fast miniature scanning probes", *J. Appl. Phys.*, vol. 98, no. 11, pp. 09, 2005.

[16]Siegfried, D. and Wilbur, P. J., "An investigation of mercury hollow cathode phenomena", *Proceedings of* 13^{th} *Int. Electric Prop. Conf.*, San Diego, California, 25-27, Apr., 1978.

[17]Albertoni, R., Rossetti, P., Paganucci, F. and Andrenucci, M. "A Reduced-Order Model for Low-Current Orificed Hollow Cathodes", *Proceedings of Space Prop. Conf.*, Bordeaux, France., vol. 7, no. 218859, 2012.

[18]Jameson, K., Goebel, D. M. and Watkins, R. M., "Hollow Cathode and Keeper-Region Plasma Measurements", *Proceedings of* 41^{st} *AIAA/ASME/SAE/ASEE Joint Prop. Conf. and Exhibit*, Tucson, Arizona, 10-13 July 2005.

[19]Jameson, K., Goebel, D. M. and Watkins, R. M., "Hollow Cathode and Thruster Discharge Chamber Plasma Measurements", *Proceedings of* 29^{th} *Int. Electric Prop. Conf., 2005*, Princeton University, Oct. 31 - Nov. 4, 2005.

[20]Hayashi, M., "Determination of Electron-Xenon Total Excitation Cross-Sections, from Threshold to 100 eV, From Experimental Values of Townsends alpha", *Journal of Physics D: Applied Physics*, Vol. 16, 1983, pp. 581589.

[21]Langmuir, I., "The interaction of electron and positive ion space charges in cathode sheaths", *Physical Review*, Vol. 33, No. 6, 1929, pp. 954-989.

[22]Domonkos, M. T., Gallimore, A. D., and Williams, G. J. J., Patterson M. J., "Low-Current Hollow Cathode Evaluation", AIAA-99-2575, 1999.

[23]Ducci, C., Oslyak, S., Dignani, D., Albertoni, R. and Andrenucci, M., "HT100D performance evaluation and endurance test results", *Proceedings of* 33^{rd} *Int. Electric Prop. Conf., IEPC2013*, Washington, D.C., 6-10, Oct., 2013.

[24]Albertoni,R., Pedrini, D., Paganucci, F. and Andrenucci, M., "Experimental Characterization of a LaB 6 Hollow Cathode for Low-Power Hall Effect Thrusters", *Space Propulsion Conference, SPC2014*, Cologne, Germany, 19-22, May, 2014.

[25]Pedrini, D., Albertoni,R., Paganucci, F. and Andrenucci, M., "Theoretical Model of a Lanthanum Hexaboride Hollow Cathode", *Proceedings of* 33^{rd} *Int. Electric Prop. Conf.*, The George Washington University, Washington, D.C., USA October 6-10, 2013.

[26]Siegfried, D. E., "A Phenomenological Model for Orificed Hollow Cathodes", Ph.D. Dissertation, Colorado State University, 1982.

[27]Siegfried, D. and Wilbur, P. J., "An investigation of mercury hollow cathode phenomena" *Proceedings of* 13^{th} *Int. Electric Prop. Conf.*, San Diego, California, USA, April 25-27, 1978.

[28]Goebel, D. M., and Katz, I., *Fundamentals of Electric Propulsion: Ion and Hall Thrusters*, John Wiley and Sons, NJ, 2008.